Article:
Stock, S, Jakob, F, Röhl, S et al. (6 more authors) (2021) Exploring water in oil emulsions simultaneously stabilized by solid hydrophobic silica nanospheres and hydrophilic soft PNIPAM microgel. Soft Matter, 17 (36). pp. 8258-8268. ISSN 1744-683X

https://doi.org/10.1039/d1sm00942g

Exploring water in oil emulsions simultaneously stabilized by solid hydrophobic silica nanospheres and hydrophilic soft PNIPAM microgel

Sebastian Stock,[a] Franziska Jakob,[a] Susanne Röhl,[b] Kevin Gräff,[a] Matthias Kühnhammer,[a] Nicole Hondow,[c] Stuart Micklethwaite,[c] Matthias Kraume[b] and Regine von Klitzing[a]

[a]Institute for Condensed Matter Physics, Technische Universität Darmstadt, Darmstadt, Germany
E-mail: klitzing@smi.tu-darmstadt.de
Tel: +49-(0)6151-16-24506
[b]Chair of Chemical and Process Engineering, Technische Universität Berlin, Berlin, Germany
[c]School of Chemical and Process Engineering, University of Leeds, Leeds, UK

Abstract
A general drawback of microgels is that they do not stabilize water-in-oil (w/o) emulsions of non-polar oils. Simultaneous stabilization with solid hydrophobic nanoparticles and soft hydrophilic microgels overcomes this problem. For a fundamental understanding of this synergistic effect the use of well defined particle systems is crucial. Therefore, the present study investigates the stabilization of water droplets in a highly non-polar oil phase using temperature responsive, soft and hydrophilic PNIPAM microgel particles (MGs) and solid and hydrophobic silica nanospheres (SNs) simultaneously. The SNs are about 20 times smaller than the MGs. In a multiscale approach the resulting emulsions are studied from the nanoscale particle properties over microscale droplet sizes to macroscopic observations. The synergy of the particles allows the stabilization of water-in-oil (w/o) emulsions, which was not possible with MGs alone, and offers a larger internal interface than the stabilization with SNs alone. Furthermore, the incorporation of hydrophilic MGs into a hydrophobic particle layer accelerates the emulsions sedimentation speed. Nevertheless, the droplets are still sufficiently protected against coalescence even in the sediment and can be redispersed by gentle shaking. Based on droplet size measurements and cryo-SEM studies we elaborate a model, which explains the found phenomena.

1 Introduction
The term particle stabilized emulsion includes emulsions stabilized by a large variety of soft and solid particles from the nano- to micrometer scale. Particle types range from solid particles like spherical[1] and non-spherical silica[2,3] over polymeric particles like polystyrene[4] and PNIPAM microgels[5–8] towards biological soft matter[9] such as proteins[10], cellulose[11] and even whole cells.[12–14] Another name predominantly used for solid particle stabilized emulsions is *Pickering emulsions* (PEs). PEs rely on the high adsorption energy of the particles at the interface, which is orders of magnitude higher than the thermal energy. This leads to an irreversible adsorption of the particles at the interface, which themselves sterically hinder the coalescence of the droplets[15]. PEs are named after S. U. Pickering[16], who together with Ramsden[17] first investigated PEs systematically at the beginning of the 20th century. For nearly one century PEs remained a niche topic with the exception of important findings by Wiley *et al.* in the 1950s[18]. At the beginning of the 21st century the interest in PEs exploded, beginning with the works of Binks *et al.*[2,4,15,19] and a vast number of

(possible) applications emerged in different disciplines such as medicine,[20–22] cosmetics[23], food industry,[24,25] material synthesis[26] and (interfacial) catalysis.[27,28]
In case of soft particles used as stabilizers, the term PE is still under debate.[29–36] In contrast to solid particles, MGs (a) deform strongly when adsorbed at the liquid/liquid interface[29,36–42] and (b) reduce the macroscopically measured interfacial tension.[36–41] To reflect these differences but also emphasize the similarities in their stabilization mechanism, the neologistic term “Mickering emulsion” (ME) was invented.[43,44] Soft particle stabilized emulsions tend to be of oil-in-water (o/w) type due to the natural hydrophilicity of most soft particle species[45]. Hydrogel particles in general and poly(*N*-isopropylacrylamide) (PNIPAM) microgels[46] in particular lack the ability to stabilize water-in-oil (w/o) type emulsions at all[47], especially, when a highly non-polar oil phase is used.[44,48] But, often the w/o type is the desired one. For example for the application of PEs (or MEs) in interfacial catalysis, the non-polar phase often constitutes or contains the substrate[49]. In this case, w/o emulsions offer the opportunity to apply low energy cost solutions for product separation, while retaining a water affine catalyst enclosed in the water droplets without the necessity of breaking the emulsion droplets.[50–52]
Different strategies emerged to overcome this problem: One strategy is the modification of the chemical structure of the MGs.[47,53] While remarkable success was made recently[53], this strategy inherently bears the disadvantage that the modifications are MG specific and may not be generalized to other types of soft particles Furthermore, for most applied MGs the inherent structure is essential for their function (*e.g.*, drug carrier MGs, proteins, *etc.*), which may suffer from the modification.
Another strategy is the use of a second species of particles to assist the stabilization. For example Jiang *et al.*[54] quite recently demonstrated the use of silica particles to assist enzyme decorated poly(2-(diethylamino)ethyl methacrylate)-based (PDEAEMA) MGs in the stabilization of w/o emulsions for catalysis. Still, the number of fundamental studies investigating the driving factors (*e.g.*, water fraction, particle mass ratio, *etc.*) and the particle–particle interaction at the interface of these multiple particle stabilized emulsions is very low. For example, Binks *et al.*[1] showed that the agglomeration of oppositely charged hydrophilic silica nanospheres (SNs) influences the o/w emulsion stability. Nallamilli *et al.*[55,56] considered these agglomerates as larger amphiphilic “particles” and modelled the emulsion stabilization by these predicting the resulting droplet sizes successfully.
Pushpam *et al.*[57] did Monte-Carlo simulations and postulated the stability of emulsions stabilized by oppositely charged particles, which may not agglomerate at the interface.
Wang *et al.*[58] investigated the droplet size of PEs stabilized simultaneously with silica and calcite particles regarding silica particle size and concentration. Griffith *et al.*[59] showed that the addition of hydrophobic silica to o/w PEs stabilized by hydrophilic silica destabilizes the emulsion.
The results of studies on emulsions with multiple stabilizers including at least one soft particle type are very diverse and disjointed: Depending on the used particle combination the introduction of a second soft stabilizing species can have an effect on the emulsion type[60] or even induce phase inversion[61]. It can reduce the PEs viscosity and reduce the shear thinning behaviour[62]. The particles can form particle bilayer[63] or the soft particles can act as a “colloidal glue” (Zembyla *et al.*[64]) between the primary stabilizer and increase the emulsion stability.[45,65,66] Often the conclusions of these studies are very particle specific due to diverging particle properties. A generalized conclusion is challenging and missing.

This is only possible with well understood and sufficiently characterized particles. Therefore, this study investigates emulsions, which were simultaneously stabilized by two common and comparably well understood model particle systems (hydrophilic, soft PNIPAM MGs and hydrophobic, solid silica nanospheres (SNs)) and aims for generalizable explanations to better understand the simultaneous stabilization. It investigates the influence of the solid/soft particle ratio and the soft particles' responsiveness on the structure of the resulting w/o emulsions. In detail, it focusses on the influence of the simultaneous stabilization on the structure formation of the particles at the w/o interface, the resulting droplet diameter and the sedimentation behaviour.
Methodically, the study represents a multi-scale approach: First, PNIPAM MGs with a positive ζ-potential are synthesized using a common and broadly studied recipe.[67–70] Hydrophobic and positively charged SNs are created from commercially available pristine particles by surface modification. The use of likely charged stabilizers makes sure that the much smaller SNs do not adsorb into the larger MGs[71]. Second, the resulting particles are characterized in detail regarding their charge, interfacial affinity and geometry. Third, emulsions were prepared with either one or both stabilizing agents. Hybrid SN/MG co-stabilized emulsions are formed from a two phase system where the two different particle types were separated initially. The hydrophobic SNs are present in the oil phase, while the hydrophilic MGs are present in the aqueous phase. During emulsification, the particles meet at the interface from opposite directions. Finally, the resulting emulsions are investigated by microscopy, droplet size analysis, cryo-SEM and sedimentation analysis and differences between simultaneously and single particle type stabilized emulsions are discussed.

2 Materials and methods

Ludox TM40 colloidal silica spheres, dimethyloctadecyl[3-(trimethoxysilyl)propyl]ammonium chloride (60% in methanol), ethanol, *N*-isopropylacrylamide (NIPAM), *N*,*N*'-methylenbisacrylamid (BIS), fluorescein sodium salt and dodecene (>96%) were purchased from Sigma-Aldrich (Merck KGaA, Darmstadt, Germany) 2,2'-azobis-2-methyl-propanimidamide dihydrochloride (AAPH) was purchased from Cayman Chemical Company (Cayman Chemical, Ann Arbor, USA). Highly purified water was used from a MiliQ purification system (Merck KGaA, Darmstadt, Germany) with a specific resistance of ρ = 18.2 MΩ cm^{-1}.

2.1 PNIPAM microgel synthesis

Microgel particles (MGs) were synthesized using a common and broadly studied recipe *via* precipitation polymerization reaction.[67–70,72] 2.15 g of *N*-isopropylacrylamide (NIPAM, monomer) and 154 mg of *N*,*N*'-methylenbisacrylamid (BIS, cross linker) were dissolved in 120 ml water. The solution was degassed in a glass reactor under constant stirring (1000 RPM) and constant nitrogen flow through the solution for at least 1 hour at 80 °C. The reaction was initiated by adding 33.5 mg 2,2'-azobis-2-methyl-propanimidamide dihydrochloride (AAPH, starter) in 1 ml water *via* a syringe and then carried out for 90 min at 80 °C and 1000 RPM. The obtained MGs were cleaned by dialysis for at least 10 days (10 cycles, 120 ml dispersion against 50 l water in total), dried by lyophilization and stored at −20 °C.

2.2 Silica nanosphere (SN) modification

Silica nanospheres (SNs) were hydrophobized similar to a procedure described in a previous work[52]. Prior to surface modification, the commercial Ludox TM40 particle solution was cleaned by dialysis for at least 10 days (10 cycles, 100 ml dispersion against 50 l water in

total). The clean suspension was diluted to 13.5 wt%. 7.5 ml of this suspension was given to 50 ml of ethanol. 0.42 ml of the silane dimethyloctadecyl[3-(trimethoxysilyl)propyl]ammonium chloride (C18n+, 60% in methanol) was diluted in another 50 ml of ethanol. The solution containing the silane was given to the particle suspension and the suspension was stirred for 1 hour at 20 °C and another 2 hours at 60 °C. After the reaction the liquid phase was evaporated completely.

2.3 Characterization of the silica nanospheres

The size of the SNs was determined from Transmission Electron Microscopy (TEM) images of a particle layer using imagej (https://imagej.net). The single particle density was calculated from the change of total density with increasing particle fraction measured with an oscillating U-tube densitometer (DM40, Mettler Toledo, USA). The particles' hydrophobicity was quantified by the determination of the contact angle of a water droplet on a spin-coated particle layer. The ζ-potential of the modified silica particles was measured with a Zetasizer Nano (Malvern Panalytical Ltd) in ethanol (0.01 wt%).

2.4 Characterization of the microgel particles (MGs)

Atomic Force Microscopy (AFM) of a spin-coated particle layer on a 2 cm × 2 cm silicon wafer (0.1 wt%, 800 RPM, 2 min) was carried out in tapping mode with a Nanowizard II (JPK, Germany) using a AC160TS (Olympus, Japan) cantilever. The hydrodynamic diameter of a diluted MG in water suspension (0.006 wt%) was measured using a commercially available Dynamic Light Scattering (DLS) setup by LS-Instruments (Switzerland). The ζ-potential was measured with a Zetasizer Nano (Malvern Panalytical, UK) in water (0.006 wt%). The MGs' interfacial activity was measured *via* Pendant Drop Tensiometry with a drop shape analyser OCA 20 (DataPhysics, Germany) with a pendant drop (0.01 wt% in the water phase, drop size 9 µl).

2.5 Emulsion preparation

The emulsions were prepared with the rotor stator mixer T25 Ultra Turrax (IKA, Germany) equipped with a S25N-10G dispersing unit at 20 kRPM for 5 minutes. The preparation temperature was adjusted by either a heat bath using a closed loop heating plate (50 °C) or a cooling bath using an unsaturated ice bath (8 °C). After preparation, the PEs were equilibrated to room temperature ((25 ± 1) °C) for 1 hour until further investigation.

2.6 (Fluorescence) microscopy and drop size determination

A drop of a few microlitres of a gently shaken emulsion was spread on an objective slide. At least 10 different images containing more than 200 droplets were taken with an Axio Imager A1 (Zeiss, Germany). For Fluorescence Microscopy the water phase was dyed prior to emulsification with water-soluble but oil-insoluble Fluorescein sodium salt (Uranin, $c = 10 \times 10^{-3}$ mmol l^{-1}). The images were taken in greyscale but coloured green in imagej for better readability. An image analysation software (SOPAT, Germany) provided the drop size distribution and the Sauter mean diameter from the (Transmission Light) Microscopy images.

2.7 Cryo-SEM

The sample was secured into a cryo shuttle by use of a freezing rivet and submerged into slushed nitrogen. The sample was then transferred under vacuum into a Quorum PP3010 cryo preparation chamber which was under high vacuum and pre-cooled to −140 °C. The sample was fractured using a cooled knife. Prior to imaging, an Iridium coating was sputtered onto the samples and it was transferred into a Thermo scientific Helios G4 CX DualBeam (Focused ion beam scanning electron microscope; FIB-SEM) operating at 1 or 2 kV and 0.1 nA. The FIB-SEM is fitted with a cold stage (−140 °C) and cold finger (−175 °C).

2.8 Sedimentation analysis

The formed w/o emulsions tend to sediment down to the bottom of the vial, leaving behind a clear oil phase completely deprived of water droplets. This leads to a characteristic intensity profile along the height of the vial. By gentle shaking, the initial dispersed state is reversible (Fig. 1A). After PE preparation the emulsions were equilibrated to room temperature for 1 hour. Then, the sedimentation behaviour was quantified by monitoring the height of the white turbid droplet containing phase relative to the total liquid height (PE fraction) over time by taking pictures with a Nikon (Japan) D7200 equipped with a TAMRON (Japan) SP 90 mm F/2.8 macro lens every 10 seconds. Afterwards, the intensity profile was extracted by image analysis for every picture. The height position of the liquid/air interphase and the turbid-clear-transition was evaluated by a low degree polynomial fit around the respective maximum/edge for every obtained intensity profile using an algorithm written in python (Fig. 1B).

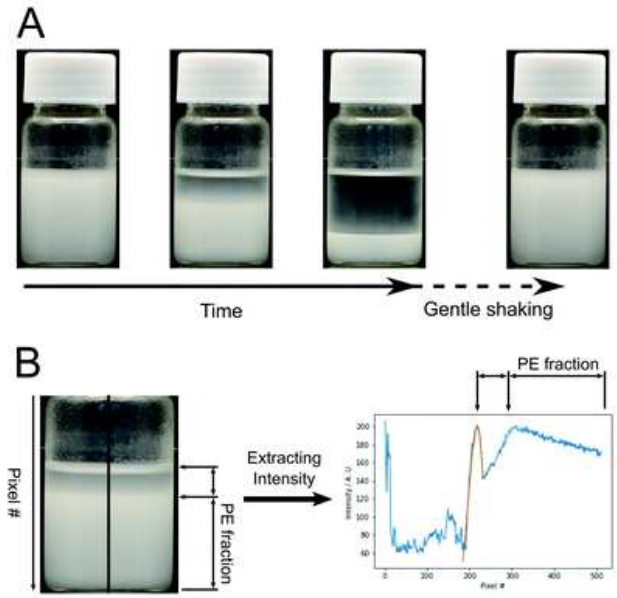

Fig. 1 (A) The presented soft/solid simultaneously stabilized emulsions are of w/o type. The water droplets in the oil phase sediment towards the bottom of the vial without breaking. Gentle shaking is sufficient to redisperse the emulsion. (B) In order to study the emulsions sedimentation behaviour, the time dependent PE fraction is evaluated from the vertical intensity profile extracted from pictures taken by a camera every 10 seconds.

3 Results

3.1 Particle characterization

Fig. 2 and Table 1 display the measured characteristic properties of the solid hydrophobized silica nanospheres (SNs). The TEM image in Fig. 2A shows the spherical shape of the SNs having a reasonably narrow and approximately symmetric size distribution with a Sauter mean diameter of around 28 nm (Fig. 2B). The single particle density was calculated from measurements of particle suspensions with different concentrations (Section S1 and Fig. S1, ESI†). With the size and the density (Table 1) a specific cross section per particle mass (a_{ϕ}) was calculated. The specific cross section is connected to the particles specific surface by a factor of 4. For more details see our previous works[52]. The contact angle of a water droplet on a particle layer is higher than 90°, *i.e.* the particles are hydrophobic. The particles are

positively charged (ζ = (56 ± 4) mV). Both, their hydrophobicity and charge, are intended results from the silanization.

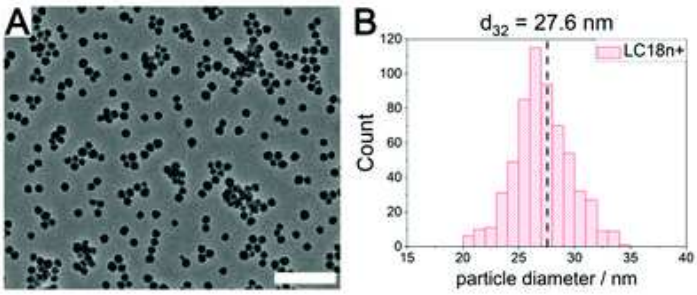

Fig. 2 Evaluation of the particle Sauter mean diameter for the hydrophobized and positively charged silica nanospheres (SNs). The white bar in the TEM-image (A) represents 200 nm. The particles have a Sauter mean diameter of 27.6 nm and the distribution has a standard deviation of ~3 nm (B).

Table 1 Overview of the SN properties: d_{32}: Sauter mean diameter from TEM; ρ_p: single particle density; $a_\varnothing$: specific cross section; $4 \cdot a_\varnothing$: specific surface.[1] measured on a particle layer,[2] in ethanol

	SNs
d_{32}/nm	27.6 ± 2.9
ρ_p/g cm^{-3}	2.15 ± 0.02
$a_\varnothing$/m^2 g^{-1}	25.3 ± 2.7
$4 \cdot a_\varnothing$/m^2 g^{-1}	101.0 ± 10.7
CA[1]/°	106 ± 8
ζ-Potential[2]/mV	+56 ± 4

Fig. 3 shows the results for the characterization of the soft microgel particles (MGs). The AFM images of these particles spin-coated on a silicon wafer (Fig. 3A) display them to be spherical with a low polydispersity. At around 35 °C, the DLS measurements of the hydrodynamic diameter (Fig. 3B) as well as the ζ-potential measurements (Fig. 3C) show the MGs going through a reversible volume phase transition (VPT) typical for PNIPAM MGs[67] (volume swelling ratio ~14.5). The ζ-potential increases with the MGs' size shrinking due to the concentration of the same amount of charged groups on a smaller surface area. Finally, the MGs' surface activity was characterized. They adsorb at the water–oil-interface and reduce the interfacial tension by roughly 25 mN m^{-1} (Fig. 3D).

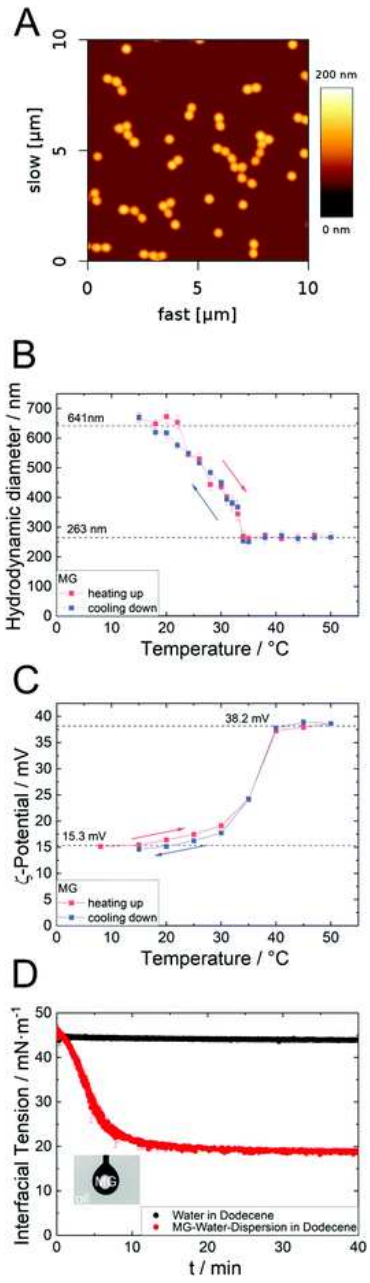

Fig. 3 Characterization of the MGs: (A) AFM micrograph of the MGs on a silicon wafer. (B) The hydrodynamic diameter of the MGs over the temperature measured by DLS. A typical and reversible VPT is observed. (C) ζ-Potential of the MGs over the temperature. It increases alongside the VPT of the MG. (D) Interfacial tension between the MG–water–solution (0.01 wt%) and dodecene over time measured by pendant drop at room temperature (25 ± 1 °C). The MGs are able to adsorb at the interface in both cases.

3.2 Emulsion characterisation

Emulsions with different soft/solid (MG/SN) particle ratios were prepared as described in Section 2.5. The total mass of particles (20 mg/~0.2 wt%) as well as the total emulsion volume of 12.55 ml and the water volume fraction (f_w = 20 vol%) were kept constant.

3.2.1 MG emulsions

Attempts to form emulsions with MGs only never resulted in the desired w/o type emulsion irrespective of preparation temperature and water volume fraction (Fig. 4). Either they formed o/w emulsions or they were unstable. Attempts to form emulsions at 8 °C with 20

vol% water fraction resulted in a two phase system, which, at first glance, looks like the initial state (Fig. 4A). A closer look by microscopy of a drop from the lower aqueous phase reveals only few very small oil droplets (Fig. 4H). With a water fraction of 40 vol% (temperature at 8 °C) a pasty emulsion phase formed (Fig. 4C). After a few hours it creamed up and a lower turbid aqueous phase appeared. Fluorescence microscopy of a drop taken from this emulsion phase reveals oil droplets in water with very strong cohesion (Fig. 4I). At 8 °C, the stirrer looks clean (Fig. 4B). At a preparation temperature of 50 °C, no emulsions formed at all neither at 20 vol% nor at 40 vol% water fraction (Fig. 4D, F and J). In both cases, the stirrer was contaminated heavily by accumulated MGs afterwards (Fig. 4E and G).

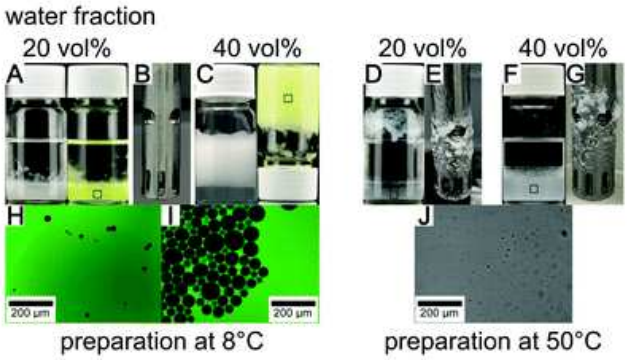

Fig. 4 Attempts to form emulsions with MGs only (m(MGs) = 20 mg, V_{tot} = 12.55 ml). Left: At 8 °C and a water fraction of 20 vol% only seldom oil droplets were observed in the water phase (fluorescence microscopy (H) with fluorescein dyed water phase of sample (A)). A pasty o/w emulsion phase was observed for a water fraction of 40 vol% (C).The photo of the sample without dye was taken ~5 h after preparation; the photo with fluorescein shows a freshly prepared emulsion. The samples contain a high amount of droplets with strong cohesion (fluorescence microscopy (I) with fluorescein dyed water phase of sample (C)). Right: At 50 °C, no emulsions formed (D, F and J) with the exception of a thin layer of very large roughly millimeter scale droplets at the w/o interfacial region for a higher water fraction (F). In both cases, a significant amount of MGs accumulated at the stirrer (E and G), which was not the case at 8 °C (B).

This may lead to the suspicion that the MGs were destroyed during the heavy stirring process. But, durability tests of MG suspensions showed that this was not the case (Fig. S2, ESI†). Fig. S2 (ESI†) shows MG suspensions stirred with 20 kRPM at 8 °C and 50 °C, respectively, in comparison to the untreated suspension. The photographs as well as the related AFM images of the MGs spin-coated on a silicon wafer show that the shearing does not harm the particles. During the stirring process, heavy foaming occurred at 8 °C but the stirrer stayed clean. At 50 °C, a low amount of foam formed but collapsed instantly. A nearly negligible but visible amount of MGs accumulates on the stirrer at the respective height where the foam collapsed.

3.2.2 SN emulsions and SN/MG emulsions

Attempts to form emulsions stabilized with only the hydrophobic SNs or stabilized simultaneously by both solid and soft particles (with 20 vol% water volume fraction) resulted always in the desired w/o emulsions (Fig. 5). All emulsions have the tendency to sediment and form a white sedimented phase after a few minutes. The droplets can easily be redispersed without damage by gentle shaking (Fig. 5A, B and Fig. S3, ESI†). The emulsion formation consumed any free water present. None of the studied emulsions containing SNs showed residual water or any unexpected deviation in the macroscopic phase structure.

Even without a detailed analysis, it is visible in the microscope images that droplet size increases with decreasing SNs mass (Fig. 5A and B) for all samples. Neither a macroscopic nor a microscopic difference was found between the emulsions with MGs prepared at 8 °C and those prepared at 50 °C.

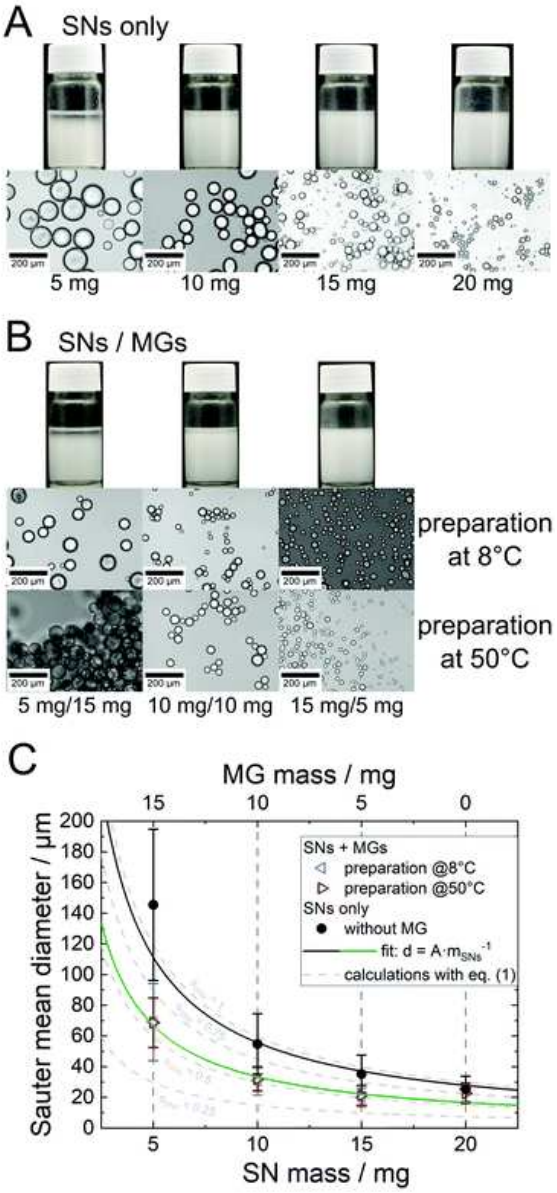

Fig. 5 (A and B) Photographs and microscopy images of w/o emulsions stabilized by SNs only and simultaneously stabilized by SNs and MGs prepared at 8 °C and 50 °C respectively but investigated at room temperature (V_{tot} = 12.55 ml, f_w = 20 vol%) in dependence on the solid particle content. The emulsions tend to sediment after a few minutes but can be redispersed by gentle shaking. (C) Sauter mean droplet diameter related to the microscopy images shown in (A and B) over the MG or SN mass. The error bars represent the standard deviation of the drop size distribution. Gray dashed lines represent calculations assuming different SN packing parameters s_{SNs} for orientation. The continuous black and green line are reciprocal fits using (1) with s_{SNs} as the free parameter.

Fig. 5C shows the Sauter mean diameter of the droplets obtained from the image analysis. The drop size analysis shows a reciprocal behaviour of the droplet size over solid nanosphere (SN) mass for both, the emulsions with and without MGs. The measured mean droplet size of PEs prepared at 8 °C and those prepared at 50 °C are very similar. To describe

the system models from classic Pickering emulsions (PEs) are applicable. For PEs in the case of limited coalescence and under the assumption that all particles adsorb at the interface, the droplet diameter is described by eqn (1):[18,52]

$$d_{PE} = \frac{V_{tot} f_w}{a_\varnothing} \cdot \frac{s_{SNs}}{m_{SNs}} \quad (1)$$

d_{PE} is the (Sauter mean) droplet diameter; V_{tot} is the total emulsion volume; f_w is the water volume fraction; $a_\varnothing$ is the specific particle cross section; s_{SNs} is the packing parameter of the solid silica nanospheres (SNs) at the interface and m_{SNs} is the total mass of solid silica nano spheres.

Except s_{SNs}, all parameters are known either from the initial phase systems composition (V_{tot}, f_w, m_{SNs}) or because they are particle specific and independently measured ($a_\varnothing$). The packing parameter $0 < s_{SNs} \leq 1$ describes the 2D coverage of the particles at the water–oil-interface. By assuming different packing scenarios (s_{SNs} = 0.25, 0.5, 0.75, 1) a set of droplet size curves can be predicted for orientation (gray dashed lines in Fig. 5C). By fitting eqn (1) to the data for the SN only stabilized emulsions, one obtains a packing parameter of $s_{SNs}(SNs_{only})$ = 0.93 ± 0.03, which is close to the theoretical 2D hexagonal close packed (hcp) parameter of $s_{hcp} \approx 0.907$. By fitting the data to the solid/soft simultaneously stabilized emulsions s_{SNs}(SNs/MGs) = 0.56 ± 0.02 was found. This includes the assumption that even in presence of MGs still nearly all solid particles adsorb at the interface.

The nanoscopic structure formation on the water–oil-interface was investigated by cryo-SEM (Fig. 6). The cryo-SEM images for the emulsion stabilized with SNs only (Fig. 6A–C) show spots where the particles are present and form a hexagonal close packed structure. On other spots the particles broke away during sample preparation. The results are in agreement on findings in previous studies with very similar particles[52].

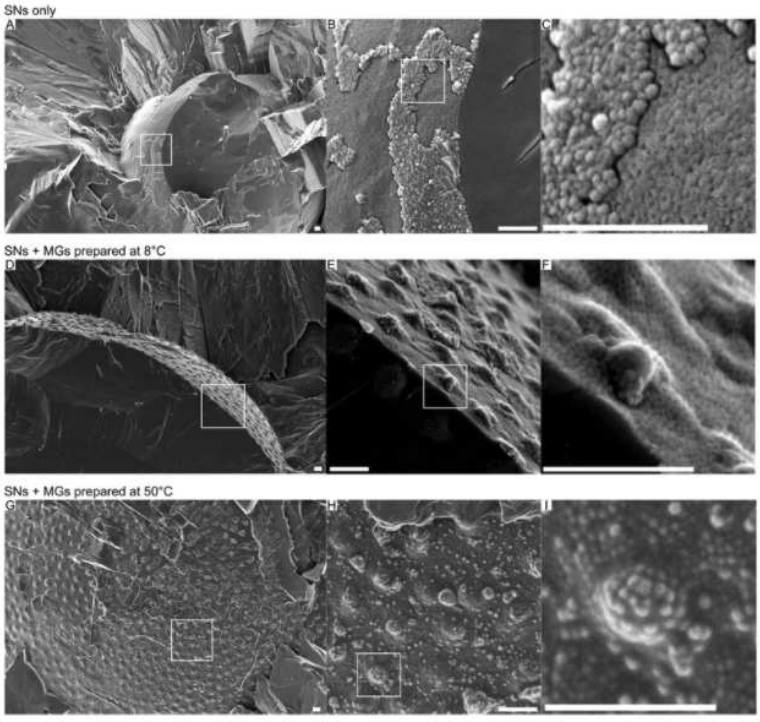

Fig. 6 Cryo-SEM images from different emulsion types. (A–C) SN only stabilized emulsion (V_{tot} = 12.55 ml, f_w = 20 vol%, m(SNs) = 20 mg). At the droplet interface spots are visible where the SNs form a crust-like structure with a close packing (presumably hcp). On other spots the particles are missing

due to the breakage in the sample preparation. (D–I) SNs/MGs simultaneously stabilized emulsions prepared at 8 °C (D–F) or 50 °C (G–I), respectively, (V_{tot} = 12.55 ml, f_w = 20 vol%, m(SNs) = 10 mg/m(MGs) = 10 mg). In case of SN/MG emulsions prepared at 8 °C the particles broke away and reveal a view on the MGs and left behind a relief-like structure. In case of SN/MG emulsions prepared at 50 °C the particle layer remained on the interface. In both cases, the MGs form a regular patterned hyperstructure (presumably hexagonal but not close), while the particles assemble around the MGs but also adsorb at their surface. The white bars represent 500 nm.

The images taken from samples prepared with both, SNs and MGs (Fig. 6D–I), proof the simultaneous adsorption at the water–oil-interface. In both cases, the MGs adsorb at the interface and form a regular patterned (presumably hexagonal) hyperstructure. The images with higher magnification for the sample prepared at 8 °C (Fig. 6E and F) shows the MGs in between the SN layer, the residuals of which can only be detected in form of the relief structure (Fig. 6F). This offers a clear view on the MGs' structure formation. In the images with higher magnification for the sample prepared at 50 °C (Fig. 6H and I), the SN layer is intact and covers the whole droplet. It shows the SNs also decorating the MGs' surface area. In summary, the SNs arrange themselves around the MGs but also adsorb at their surface. Differences between the preparation at 8 °C and 50 °C are not evident, which is in agreement with the drop size distribution measurements. The interfacial structure formation looks in both cases very similar.

3.3 Sedimentation analysis

Fig. 7(A–C) shows the PE fraction over time. We found that the PE fraction shows a single exponential decay:

$$f_{PE} = A \cdot e^{-Bt} + C \tag{2}$$

f_{PE} is the emulsion (PE) volume fraction, A is the amplitude ($f_{PE}(t = 0) - C$), B the sedimentation rate and C the final PE volume fraction.

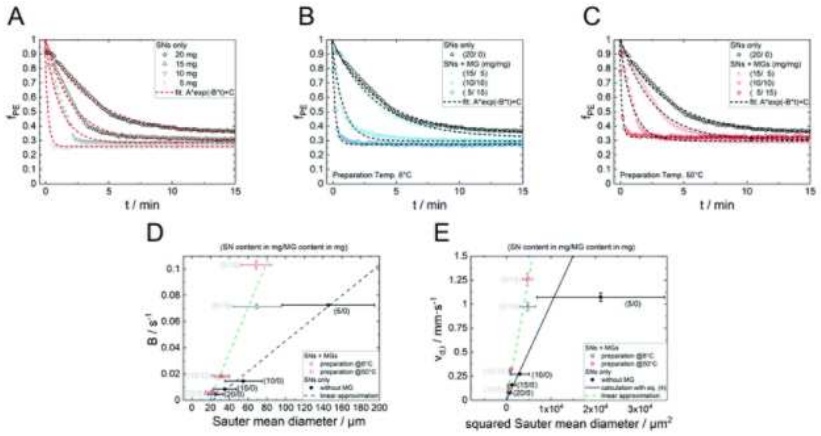

Fig. 7 Sedimentation curves (PE volume fraction over time) of the different emulsions (V_{tot} = 12.55 ml, f_w = 20 vol%, at room temperature). The PE volume fraction was evaluated from a series of photos taken every 10 seconds. (A) Prepared with SNs only (B) prepared with SNs and MGs at 8 °C (C) prepared with SNs and MGs at 50 °C (D) sedimentation rate determined from the fit of a simple exponential decay plotted against the droplet diameter. (E) Initial drift velocity calculated with eqn (3) over the squared Sauter mean droplet diameter. The emulsions stabilized with MGs sediment faster than emulsions without MGs relative to their droplet size.

Eqn (2) describes the data well and the obtained parameter *B* characterizes the sedimentation time and therefore was called sedimentation rate. *B* is linearly connected to the initial drift velocity $v_{d,i}$ *via* eqn (3):

$$v_{d,i} = h \cdot \frac{d}{dt} f_{PE}(t=0) = -A \cdot B \cdot h \quad (3)$$

h is the total emulsion height. The drift velocity of a single (solid) sphere with density ρ_P and diameter *d* in a medium with a density ρ_l and a dynamic viscosity η at low Reynolds numbers under the gravitational force (*g*: gravitational constant) is given by the Stokes equation (derivation see for example Pal *et al.*[73]):

$$v_{d,Stokes} = \frac{1}{18} \frac{d^2 \cdot (\rho_P - \rho_l)}{\eta} \quad (4)$$

It was found that the sedimentation rate *B* shows a linear dependence on the droplet size for both types of stabilization (Fig. 7D). But, the emulsions stabilized with SNs and MGs simultaneously sedimented relative to their droplet size faster than the PEs stabilized with SNs only. The case is similar for the initial drift velocity (Fig. 7E): while the curve for the single-sphere drift velocity (calculated from eqn (4)) describes the data for the emulsions with SNs only quite well, the data for the SN/MG emulsions systematically lays higher than expected *i.e.* they even start their sedimentation faster.

4 Discussion

The particle characterization (Section 3.1) shows that both particle types are positively charged in polar solvents. The MGs are hydrophilic, while SNs are hydrophobic. Besides their differences in amphilicity, MGs and SNs differ strongly in size. The soft MGs are 10–20× larger than the solid SNs.

When it comes to PE formation, both particles follow their nature. The hydrophilic MGs tend to form o/w emulsions, while the hydrophobic SNs form w/o emulsions. But there is more to learn from the attempts to form emulsions with MGs only, because their ability to stabilize emulsions has a water phase fraction dependent and a temperature-dependent component. For some types of amphiphilic particles and some specific oil types a phase inversion may occur when lowering the water volume fraction, *e.g.*, fumed silica in water–toluene emulsions[19]. But, the observed tendency that the number of droplets decreases drastically with decreasing the water fraction from 40 vol% to 20 vol% (Fig. 4A and C) indicates that a phase inversion is not possible with the present MGs and the used highly non-polar oil. The strong adhesion between the droplets for the water fraction of 40% was investigated already in detail by Destribats *et al.*[74] and originates from particle bridging, *i.e.*, two or more droplets share the same MG.

The increase in preparation temperature above the volume phase transition temperature of the MG prevents the formation of any emulsion phase (Fig. 4D, F and J). The temperature induced collapse of emulsions and foams was already studied in detail by various authors.[42,49,75] The explanation in the present case may be described as the following: While MGs still may attach to the interface created by stirring, the shrunken MGs are not able to protect the emulsion from coalescence effectively. This leads to an instant and strong coalescence of freshly formed droplets. The MGs attached to the coalescing droplets are rather pushed out of the interface or are increasingly deprived of their free space at the interface. This later case may be comparable to the situation of a MG layer on the 2D interface on a Langmuir–Blodgett–Trough. Under compression of the interface the MGs

tend to be squeezed together and crowding effects occur[76]. Therefore, the MGs – now in close contact to each other – agglomerate and accumulate only at the height of the stirrer where the emulsion droplets are formed by sheering and instantly collapse (Fig. 4E and G). The same effect may explain the contamination of the upper part of the stirrer during the MGs' durability tests at 50 °C. In this case, the foam formed from stirring induced air bubbles at the water–surface collapses instantly and the MGs – now in close proximity to each other at the interface – agglomerate and accumulate at the upper part of the stirrer (Fig. S2, ESI). Similar flocculation has been observed by Wiese *et al.*[49] when intentionally destroying PNIPAM MGs stabilized emulsions prepared at room temperature by raising the temperature.

The results change fundamentally when replacing at least 25% of the MG mass with hydrophobic SNs. The preparation temperature in this case does not play a role anymore. The presence of SNs results in the w/o type in every SN/MG stabilized emulsion that was investigated and the MGs did not agglomerate at the stirrer irrespective of the temperature. Independent from the MG proportion a constant relative shift towards smaller droplet sizes is observed when comparing the PEs with MGs towards those without MGs (Fig. 5C). This leads to the conclusion that the MGs are incorporated at the interface structure and stabilize additional interface. Both, the SN stabilized and the SN/MG stabilized emulsions show a reciprocal dependence of the SN mass but no visible correlation with the MG mass – besides the relative decrease in droplet size. This indicates that only a constant relative amount of MGs is incorporated at the interface in dependence of the present number of SNs. Or *vice versa*, there has to be a sufficient amount of SNs per MG present at the interface. This raises the suspicion that for every MG containing sample (even for the lowest MG concentration) more MG is present than the amount that can be incorporated at the interface. This means a significant amount of excess MG remains in the bulk of the droplets, while only some are integrated into the interface by the SNs. In detail, the much smaller SNs assemble around the MGs, protecting them from being squeezed or pushed out of the interface and take over the duty of coalescence hindrance (see Fig. 8A). So it is reasonable to assume that while not all MGs attach to the interface, nearly all SNs do, because the MGs rely on them acting as their stabilizing assistants.

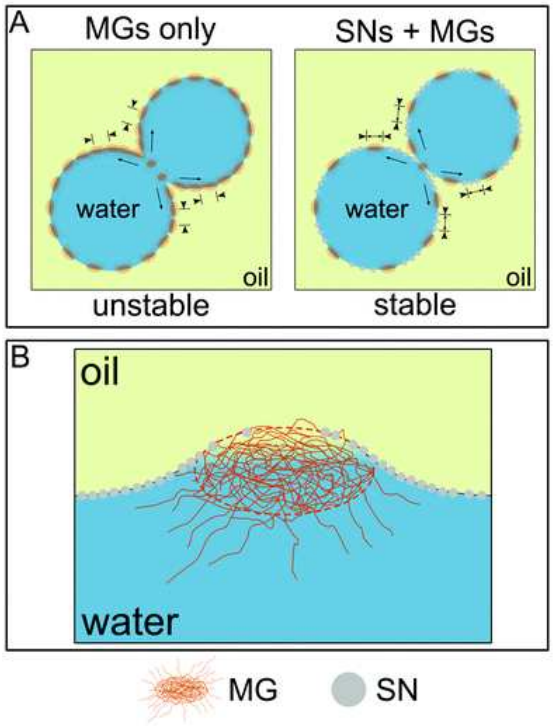

Fig. 8 Illustration of the proposed stabilization mechanism for MG/SN stabilized emulsions at the droplet interface in the nano/micrometer regime. (A) The solid and hydrophobic particles attach to the interface from the oil phase, while the hydrophilic MGs attach to the interface from the aqueous phase. Both, the SNs and the MGs adsorb at the interface. SNs are also able to adsorb onto the MGs. (B) This results in protecting shell formation of SNs in the 2D layer around the MGs. MGs alone cannot protect the droplets from coalescence, but the combination of SNs and MGs can.

Assuming all SNs adsorbing at the interface in presence and absence of the MGs enables the calculation of a SN packing parameter for both cases: this results for SN stabilized emulsions in s_{SNs}(SNs) = 0.93 ± 0.03 and is lowered for SN/MG stabilized emulsions to s_{SNs}(SNs/MGs) = 0.56 ± 0.02. This means with respect to the model above that (a) the MGs stabilize additional interface or act as a “spacer” for the SNs (decrease from s_{SNs}(SNs) = 0.93 to s_{SNs}(SNs/MGs) = 0.56) but at least ~56% (s_{SNs}(SNs/MGs)) of the droplets surface needs to be covered with SNs for stable emulsion formation.
This model is backed up by the observations in the cryo-SEM studies. The emulsion droplets stabilized by SNs only, in agreement with earlier studies[52] posses a hexagonal close packed layer of SNs at the interface (Fig. 6A–C). This is reflected by the fits of the droplet size curves, which resulted in s_{SNs}(SNs) = 0.93 ± 0.03 ≈ s_{hcp}. The images of the droplet interface of the SN/MG stabilized emulsions show the larger MGs forming a presumably hexagonal patterned hyperstructure (Fig. 6D–I), in-between which the smaller SNs adsorb at the interface or in other words form 2D-shells around the MGs, resulting in the reduction of the SNs' packing parameter. The situation for one MG surrounded by some SNs is shown in Fig. 8B.
It remains speculative which force results in the particles attaching to MG surface coming from the oil phase and why the charge of the particles is not preventing it. But, it may be explained by the following: It is typical for highly non-polar solvents (like the used one) that particles in it are less charged due to the high energy cost.[52,77] In the present case, the low ζ-potential of the MGs in water should completely vanish in the oil phase. Also the mediocre ζ-potential of the SNs is presumably reduced there. Therefore, a random

attachment at the surface of the MGs seems plausible. This attachment of the hydrophobic SNs onto the hydrophilic MGs may even be energetically favourable, since the energetically unfavourable MG/dodecene interface is replaced by a presumably preferable SN/dodecene interface.
Besides the deviation in droplet size, the SN/MG stabilized emulsions differ from SN stabilized ones in their sedimentation behaviour. Fig. 7D shows that for both emulsion types a nearly linear dependence of the sedimentation rate over the droplet diameter was found, but the slope in case of SN/MG stabilized emulsions is significantly steeper. Also the initial sedimentation speed $v_{d,i}$ is higher (Fig. 7E). This means that SN/MG stabilized emulsions sediment faster relative to their droplet diameter. Since every outer emulsion parameter was held constant and no coalescence was observed, a reasonable explanation is that the droplets that contain MGs are (a) more prone to particle bridging and/or (b) less prone to surround themself with the oil molecules, *i.e.*, the emulsions are enthalpically less stable against sedimentation and/or (c) are easier to deform. (a) Even if no undeniable proof of particle bridging was observed during microscopy this is a commonly observed effect for emulsions stabilized by comparably large and fluffy MGs[31] and would also explain the strong droplet cohesion in the emulsions prepared with MGs only at 8 °C. These bridged droplets may then act as larger "droplets", which themselves sediment faster due to their larger size. (b) An additional explanation may be found in the enthalpy of the system. Considering the lower percentage of hydrophobic SNs and the *vice versa* higher amount of hydrophilic MGs at the interface for SN/MG stabilized emulsions, compared with the SN only stabilized ones, may lead to an overall lower hydrophobicity of the droplets. This leads to a lower affinity of the droplets to surround themselves with oil molecules and, as a result, to drop out of the oil phase faster. Pal[73] suggested in his work that the sedimentation/creaming drift velocity of the droplets is dependent on their contact angle, *i.e.*, their hydrophobicity, which may explain the observed behaviour here. (c) The influence of the deformability of droplets may also have an effect on the droplets sedimentation behaviour. Since the droplets containing MG may be more elastic relative to their droplet size this could have an effect on their fluid mechanics. Faulde *et al.*[78] found this dependence for droplets in the milimeter scale, but the transfer of their models on droplets in the micrometer scale stays speculative.

5 Conclusions

Adding hydrophobic SNs to the MG–water–oil system enables the formation of w/o emulsions, which is not possible using MGs only. The droplet size of these SN/MG stabilized emulsions is significantly smaller than for SN only stabilized emulsions, but is governed exclusively by the absolute SN concentration for all investigated MG/SN ratios. It was calculated that an area of ~56% of the droplets surface is covered by SNs. This may be considered as the minimum coverage by hydrophobic material necessary for a stable w/o emulsion. The excess of MGs remains trapped in the droplet bulk. Despite we showed that the used PNIPAM MGs are temperature responsive in their size and charge, the preparation temperature had no influence on any measured emulsion property when investigating the systems after preparation at room temperature: Even if there was an effect of temperature during preparation, the system is reversible afterwards. The cryo-SEM studies of the emulsions revealed the structure formation at the interface: the SNs are located at the interface between the MGs in a very dense packing (presumably hcp) but also adsorbed on their surface in a very lose packing. The use of SNs to enables the stabilization of w/o emulsions with hydrophilic particles present is an easy, convenient and economic strategy

to achieve the preferred formation of w/o type emulsions with hydrophilic particles. The new and detailed insights as well as the proposed models provide crucial information for the better understanding of any application where soft hydrophilic particles meet solid hydrophobic ones at the interface of w/o droplets, *e.g.*, in the PE assisted interfacial catalysis.

Conflicts of interest

There are no conflicts to declare.

Acknowledgements

The authors thank Marcus Witt for providing the TEM images of the SNs and Olaf Soltwedel for proof reading. Funded by Engineering and Physical Sciences Research Council (EPSRC), UK under grants EP/P00122X/1 and EP/R043388/1. Gefördert durch die Deutsche Forschungsgemeinschaft (DFG) – TRR 63 “Integrierte chemische Prozesse in flüssigen Mehrphasensystemen” (Teilprojekt B6) – 56091768. Funded by the Deutsche Forschungsgemeinschaft (DFG, German Research Foundation) – TRR 63 “Integrated Chemical Processes in Liquid Multiphase Systems” (subproject B6) – 56091768.

Notes and references

1. B. P. Binks , W. Liu and J. A. Rodrigues , Langmuir, 2008, 24 , 4443 —4446.
2. B. P. Binks and S. O. Lumsdon , Phys. Chem. Chem. Phys., 1999, 1 , 3007 —3016.
3. A. Drelich , F. Gomez , D. Clausse and I. Pezron , Colloids Surf., A, 2010, 365 , 171 —177.
4. B. P. Binks and S. O. Lumsdon , Langmuir, 2001, 17 , 4540 —4547 .
5. T. Ngai , S. H. Behrens and H. Auweter , Chem. Commun., 2005, 331 —333.
6. T. Ngai , H. Auweter and S. H. Behrens , Macromolecules, 2006, 39 , 8171 —8177 .
7. B. Brugger , B. A. Rosen and W. Richtering , Langmuir, 2008, 24 , 12202 —12208 .
8. S. Tsuji and H. Kawaguchi , Langmuir, 2008, 24 , 3300 —3305.
9. A. Sharkawy , M. F. Barreiro and A. E. Rodrigues , Carbohydr. Polym., 2020, 250 , 116885 .
10. Y. Xi , B. Liu , H. Jiang , S. Yin , T. Ngai and X. Yang , Chem. Sci., 2020, 11 , 3797 —3803.
11. L. Bai , S. Huan , W. Xiang and O. J. Rojas , Green Chem., 2018, 20 , 1571 —1582.
12. Z. Chen , H. Ji , C. Zhao , E. Ju , J. Ren and X. Qu , Angew. Chem., Int. Ed., 2015, 54 , 4904 —4908 .
13. R. Röllig , C. Plikat and M. B. Ansorge-Schumacher , Angew. Chem., 2019, 131 , 13094 —13097.
14. H. Xie , W. Zhao , D. C. Ali , X. Zhang and Z. Wang , Catal. Sci. Technol., 2021, 11 , 2816 —2826.
15. B. P. Binks Curr. Opin. Colloid Interface Sci., 2002, 7 , 21 —41.
16. S. U. Pickering J. Chem. Soc., Trans., 1907, 91 , 2001 —2021.
17. W. Ramsden Royal Society, 1904, 477 —486.
18. R. Wiley J. Colloid Sci., 1954, 9 , 427 —437.
19. B. P. Binks and S. O. Lumsdon , Langmuir, 2000, 16 , 2539 —2547.
20. J. Marto , A. Ascenso , S. Simoes , A. J. Almeida and H. M. Ribeiro , Expert Opin. Drug Delivery, 2016, 13 , 1093 —1107.

21. C. L. Harman , M. A. Patel , S. Guldin and G.-L. Davies , Curr. Opin. Colloid Interface Sci., 2019, 39 , 173 —189.
22. K. Chen , Y. Qian , C. Wang , D. Yang , X. Qiu and B. P. Binks , J. Colloid Interface Sci., 2021, 591 , 352 —362.
23. F. G. Hougeir and L. Kircik , Dermatol. Ther., 2012, 25 , 234 —237.
24. B. S. Murray Curr. Opin. Food Sci., 2019, 27 , 57 —63.
25. A. Sarkar and E. Dickinson , Curr. Opin. Colloid Interface Sci., 2020, 49 , 69 —81 .
26. L. Ye , T. Zhou and X. Shen , Mol. Imprint., 2015, 3 , 257.
27. M. Pera-Titus , L. Leclercq , J.-M. Clacens , F. de Campo and V. Nardello-Rataj , Angew. Chem., Int. Ed., 2015, 54 , 2006 —2021 .
28. A. M. B. Rodriguez and B. P. Binks , Soft Matter, 2020, 10221 —10243.
29. M. Destribats , V. Lapeyre , M. Wolfs , E. Sellier , F. Leal-Calderon , V. Ravaine and V. Schmitt , Soft Matter, 2011, 7 , 7689.
30. V. Schmitt and V. Ravaine , Curr. Opin. Colloid Interface Sci., 2013, 18 , 532 —541.
31. M. Destribats , M. Eyharts , V. Lapeyre , E. Sellier , I. Varga , V. Ravaine and V. Schmitt , Langmuir, 2014, 30 , 1768 —1777.
32. M.-C. Tatry , P. Galanopoulo , L. Waldmann , V. Lapeyre , P. Garrigue , V. Schmitt and V. Ravaine , J. Colloid Interface Sci., 2020, 589 , 96 —109.
33. W. Richtering Langmuir, 2012, 28 , 17218 —17229.
34. Z. Li , D. Harbottle , E. Pensini , T. Ngai , W. Richtering and Z. Xu , Langmuir, 2015, 31 , 6282 —6288.
35. M.-h. Kwok and T. Ngai , J. Taiwan Inst. Chem. Eng., 2018, 92 , 97 —105.
36. I. Navarro Arrebola , L. Billon and G. Aguirre , Adv. Colloid Interface Sci., 2021, 287 , 102333.
37. F. Pinaud , K. Geisel , P. Massé , B. Catargi , L. Isa , W. Richtering , V. Ravaine and V. Schmitt , Soft Matter, 2014, 10 , 6963 —6974.
38. Z. Li , W. Richtering and T. Ngai , Soft Matter, 2014, 10 , 6182 —6191.
39. R. W. Style , L. Isa and E. R. Dufresne , Soft Matter, 2015, 11 , 7412 —7419.
40. M.-h. Kwok and T. Ngai , Front. Chem., 2018, 6 , 148.
41. M.-h. Kwok , G. Sun and T. Ngai , Langmuir, 2019, 35 , 4205 —4217.
42. M. Rey , M. A. Fernandez-Rodriguez , M. Karg , L. Isa and N. Vogel , Acc. Chem. Res., 2020, 53 , 414 —424.
43. M. A. Fernandez-Rodriguez , A. Martín-Molina and J. Maldonado-Valderrama , Adv. Colloid Interface Sci., 2021, 288 , 102350.
44. S. Schmidt , T. Liu , S. Rütten , K.-H. Phan , M. Möller and W. Richtering , Langmuir, 2011, 27 , 9801 —9806.
45. M. Zembyla , A. Lazidis , B. S. Murray and A. Sarkar , J. Food Eng., 2020, 281 , 109991.
46. R. Pelton J. Colloid Interface Sci., 2010, 348 , 673 —674.
47. T. Watanabe , M. Takizawa , H. Jiang , T. Ngai and D. Suzuki , Chem. Commun., 2019, 55 , 5990 —5993.
48. M. Destribats , V. Lapeyre , E. Sellier , F. Leal-Calderon , V. Schmitt and V. Ravaine , Langmuir, 2011, 27 , 14096 —14107.
49. S. Wiese , A. C. Spiess and W. Richtering , Angew. Chem., Int. Ed., 2013, 52 , 576 —579.
50. M. V. Kempin , S. Stock , R. von Klitzing , M. Kraume and A. Drews , Sep. Purif. Technol., 2020, 252 , 117457.

51. M. V. Kempin , M. Kraume and A. Drews , J. Colloid Interface Sci., 2020, 573 , 135 —149.
52. S. Stock , A. Schlander , M. Kempin , R. Geisler , D. Stehl , K. Spanheimer , N. Hondow, S. Micklethwaite , A. Weber , R. Schomäcker, A. Drews , M. Gallei and R. von Klitzing, Phys. Chem. Chem. Phys., 2021, 23 , 2355 —2367.
53. T. Zhang and T. Ngai , Langmuir, 2021, 37 , 1045 —1053.
54. H. Jiang , L. Liu , Y. Li , S. Yin and T. Ngai , ACS Appl. Mater. Interfaces, 2020, 12 , 4989 —4997.
55. T. Nallamilli , E. Mani and M. G. Basavaraj , Langmuir, 2014, 30 , 9336 —9345.
56. T. Nallamilli , B. P. Binks , E. Mani and M. G. Basavaraj , Langmuir, 2015, 31 , 11200 —11208.
57. S. D. C. Pushpam , M. G. Basavaraj and E. Mani , Physical Review E, 2015, 92 , 5.
58. S. Wang , Y. He and Y. Zou , Particuology, 2010, 8 , 390 —393.
59. C. Griffith and H. Daigle , J. Colloid Interface Sci., 2019, 547 , 117 —126.
60. H. Cheng , H. Zhang , D. Li , H. Duan and L. Liang , Food Hydrocolloids, 2020, 109 , 106119.
61. S. B. Ogunlaja , R. Pal and K. Sarikhani , Canadian J. Chem. Eng., 2018, 96 , 1089 —1097.
62. A. Heyse , M. Kraume and A. Drews , Colloids Surf., B, 2020, 185 , 110580.
63. S. Tao , H. Jiang , R. Wang , C. Yang , Y. Li and T. Ngai , Chem. Commun., 2020, 56 , 14011 —14014.
64. M. Zembyla , A. Lazidis , B. S. Murray and A. Sarkar , Langmuir, 2019, 35 , 13078 —13089.
65. M. Zembyla , B. S. Murray , S. J. Radford and A. Sarkar , J. Colloid Interface Sci., 2019, 548 , 88 —99.
66. S. Zhang , B. S. Murray , N. Suriyachay , M. Holmes , R. Ettelaie and A. Sarkar , Langmuir, 2021, 37 , 827 —840.
67. R. Pelton Adv. Colloid Interface Sci., 2000, 85 , 1 —33.
68. T. Hoare and R. Pelton , Macromolecules, 2004, 37 , 2544 —2550.
69. A. Garcia , M. Marquez , T. Cai , R. Rosario , Z. Hu , D. Gust , M. Hayes , S. A. Vail and C.-D. Park , Langmuir, 2007, 23 , 224 —229.
70. N. Sanson and J. Rieger , Polym. Chem., 2010, 1 , 965.
71. M. U. Witt , S. Hinrichs , N. Möller , S. Backes , B. Fischer and R. von Klitzing , J. Phys. Chem. B, 2019, 123 , 2405 —2413.
72. R. H. Pelton and P. Chibante , Colloids Surf., 1986, 20 , 247 —256 .
73. R. Pal Fluids, 2019, 4 , 186.
74. M. Destribats , V. Lapeyre , E. Sellier , F. Leal-Calderon , V. Ravaine and V. Schmitt , Langmuir, 2012, 28 , 3744 —3755.
75. Y. Horiguchi , H. Kawakita , K. Ohto and S. Morisada , Adv. Powder Technol., 2018, 29 , 266 —272.
76. A. Rauh , M. Rey , L. Barbera , M. Zanini , M. Karg and L. Isa , Soft Matter, 2016, 13 , 158 —169.
77. J. Lee , Z.-L. Zhou , G. Alas and S. H. Behrens , Langmuir, 2015, 31 , 11989 —11999.
78. M. Faulde , E. Siemes , D. Wöll and A. Jupke , Polymers, 2018, 10 , 809.